Chinese Chemical Letters 37 (2026) 111991

Contents lists available at ScienceDirect

Chinese Chemical Letters

journal homepage: www.elsevier.com/locate/cclet

Molecularly-engineered zwitterionic micelles for adaptive lubrication

Yihan Fu[a,b], Xinyi Wang[a,b], Sen Li[a,b], Weifeng Lin[a,b,*], Mingjie Liu[a,b,*]

[a] State Key Laboratory of Bioinspired Interfacial Materials Science, Bioinspired Science Innovation Center, Hangzhou International Innovation Institute, Beihang University, Hangzhou 311115, China
[b] State Key Laboratory of Bioinspired Interfacial Materials Science, School of Chemistry, Beihang University, Beijing 100191, China

ARTICLE INFO

Article history:
Received 9 July 2025
Revised 15 October 2025
Accepted 20 October 2025
Available online 22 October 2025

Keywords:
Zwitterionic surfactant
Substrate-adaptable
Dual-responsive
Hydration lubrication
Lubricant additive

ABSTRACT

Water-based lubrication systems incorporating nanoparticles as highly promising additives are of great importance for enabling sustainable and environmentally benign tribological solutions. However, persistent limitations encompass pronounced substrate dependence, inadequate dynamic responsiveness under operating conditions, and intrinsically constrained lubrication performance, collectively impeding their transition from laboratory potential to robust industrial deployment. To tackle these challenges, we have developed a substrate-adaptable and dual-responsive lysine-based surfactant (LBS) as a cutting-edge water-based lubrication additive. LBS achieves substrate-independent adsorption through multiple interactions between its head group and substrates of varying properties. LBS maintains consistent lubrication performance with minimal COF variation across substrates with divergent surface charges, confirming its adaptability to diverse tribological substrates. Notably, the engineered surfactant demonstrates outstanding lubricating properties, achieving a coefficient of friction (COF) of ~0.06 under extreme pressure condition (~500 MPa), a 95 % reduction in COF compared to pure water and maintaining stable lubrication over 25,000 cycles without significant wear or interfacial degradation. Additionally, by leveraging the pH sensitivity of the molecular structure and the temperature responsiveness of the micellar assembly, the COF can be rapidly modulated over a 10-fold range in response by changes pH and temperature. By synergistically integrating universal substrate adaptability with stimuli-responsive behavior, this work not only ensures stable lubrication in complex substrates, but also opens new avenues for the intelligent design of surfactants, offering significant potential for large-scale applications in intelligent lubrication.

© 2026 Published by Elsevier B.V. on behalf of Chinese Chemical Society and Institute of Materia Medica, Chinese Academy of Medical Sciences.

Water-based lubrication has evolved into fundamentally efficient lubricating mechanism in friction system [1], due to its low viscous losses, efficient heat transfer, and excellent biocompatibility [2,3]. Its effectiveness relies on maintaining sub-nanometer-scale hydration shells at sliding interfaces. During the friction process, water molecules are exchanged rapidly in the hydration layers to achieve dynamic equilibrium, which can significantly reduce friction dissipation [4,5]. To increase the stability of water-based lubrication under high speed or high load friction conditions, the formation and characteristics of water-based lubricating films at friction interfaces critically determine system performance by minimizing direct surface contact [6–8]. The functional architecture of water-based lubrication films, nanoscale interfacial layers (1 to a few tens of nanometers) formed through physical adsorption or chemical bonding [9], is governed by key tribological components, including nanoconfined hydrated ions [10], surfactants [11–13], high hydrated polymers [14,15], and phosphatidylcholine (PC) vesicles [16]. These elements operate through interfacial hydration engineering, unified by the presence of hydration-active moieties at the tribological interface that enable ultralow friction coefficients *via* persistent boundary lubrication regimes [17]. Surfactants exhibit remarkable diversity in their chemical structures and demonstrate exceptional lubrication capabilities, where cationic and anionic surfactants enhance interfacial lubrication performance through selective adsorption onto oppositely charged surfaces *via* electrostatic interaction, thereby reducing friction and wear [7]. However, conventional single-ionic surfactants such as anionic sodium dodecyl sulfate (SDS) or cationic cetyltrimethylammonium bromide (CTAB) [18] face inherent limitations due to pronounced substrate specificity [19], where cationic surfactants predominantly adsorb on electronegative surfaces such as mica and silica [1,20], while anionic surfactants are restricted to electropositive surfaces such as Al_2O_3 and amine-functionalized surfaces. This material-dependent adsorption behavior creates significant challenges in developing universal lubrication solutions across diverse material interfaces [21,22]. Additionally, with the growing demand

* Corresponding authors.
E-mail addresses: linwf@buaa.edu.cn (W. Lin), liumj@buaa.edu.cn (M. Liu).

https://doi.org/10.1016/j.cclet.2025.111991
1001-8417/© 2026 Published by Elsevier B.V. on behalf of Chinese Chemical Society and Institute of Materia Medica, Chinese Academy of Medical Sciences.

for smart lubrication systems with environmental responsiveness has driven research toward stimuli-adaptive surfactants capable of converting electrical [23], optical, thermal [24], or pH stimuli [25] into precisely modulated tribological responses [26]. Such advanced surfactants require engineered molecular architectures enabling rapid, reversible modulation of interfacial properties without compromising structural integrity through decomposition or phase separation, thereby necessitating enhanced thermodynamic stability and robust molecular design to meet the transition from laboratory potential to robust industrial deployment [27,28]. To address these challenges, biocompatible zwitterionic materials have recently attracted extensive attention in the area of bio-lubrication [23,29], which is an important motivation also for the present study.

This study introduces a substrate adaptability and environmentally responsive surfactant as a water-based lubrication additive featuring an amino acid-based zwitterionic surfactants engineered for various friction substrate change and agile lubrication performance controllable. Lysine employed as the functional headgroup, a series of lysine-based surfactants (LBS) were synthesized with different headgroup configurations and tail lengths to systematically optimize lubrication performance. The molecular architecture of LBS facilitates the formation of high-strength interfacial physical adsorption films on the diverse friction pair surface, establishing stable hydration lubricating layers than maintain coefficient of friction (COF) below 0.10 across from 100 MPa to 500 MPa. The zwitterionic headgroup ensures exceptional substrate adaptability owing to the multiple interactions between the head base and the substrate, which include electrostatic interaction, ionic dipole interaction, hydrogen bond, van der Waals force, *etc*. These enable robust lubrication performance on negative charged, uncharged positive charged and hydrophobic substrate. In addition, temperature and pH dual stimuli enable reversible, order-of-magnitude modulation (>10-fold) of COF values, achieving precise tribological control. The synergistic combination of broad substrate compatibility, dual-stimuli responsiveness (thermal/pH), low-viscosity fluid dynamics, and inherent biocompatibility positions LBS as a transformative solution for advanced lubrication systems requiring adaptive performance under variable operational conditions.

The lysine molecule featuring two amino groups, an α-amino group ($pK_a = 8.95$) and an aliphatic ε-amino group ($pK_a = 10.67$), exhibits high structural versatility and molecular design flexibility. To identify optimal configurations for enhanced lubrication, a series of lysine-derived zwitterionic surfactants were systematically designed with variations in headgroup geometry (α- *vs.* ε-configuration) and hydrophobic tail length (alkyl chains: $n = 8$, 10, 12), designated as *n*-α and *n*-ε, to reflect the specific amino group functionalization (Fig. 1a). Computational analysis of the electrostatic potential of the two headgroups revealed that in the *n*-α configuration, spatial proximity between the amino and carboxyl groups induces significant intramolecular complexation (Fig. 1b), which critically compromises aqueous solubility-even the shortest-chain 8-α demonstrates complete water insolubility, in stark contrast to the fully soluble 8-ε, thereby limiting the applicability of *n*-α in aqueous lubrication systems (Fig. 1c). In the *n*-ε configuration, the amino and carboxyl groups are separated by four methylene groups, resulting in relatively weak intramolecular interactions compared to the *n*-α configuration. This structural distinction endows the *n*-ε with markedly higher aqueous solubility than the *n*-α, making it a superior candidate for water-based lubricants. Moreover, this elongated molecular spacing not only not only mitigates charge neutralization effects but also confers enhanced rotational freedom to the headgroup, enabling the ε-configuration to dynamically adapt its spatial orientation across diverse chemical environments. Such structural flexibility facilitates robust adsorption on both electronegative and electropositive surfaces through dual-mode charge interactions, overcoming the substrate selectivity limitations inherent to conventional surfactants (Fig. 1d). Thus, the ε conformation of LBS is particularly well-suited as the configuration of lubricating additive, which will be further explored subsequently. Furthermore, the nanoscale aggregation behavior and headgroup charge characteristics of LBS demonstrate rapid, reversible structural reorganization in response to thermal or pH stimuli, endowing the lubrication system with dual-stimuli responsiveness (Fig. 1e).

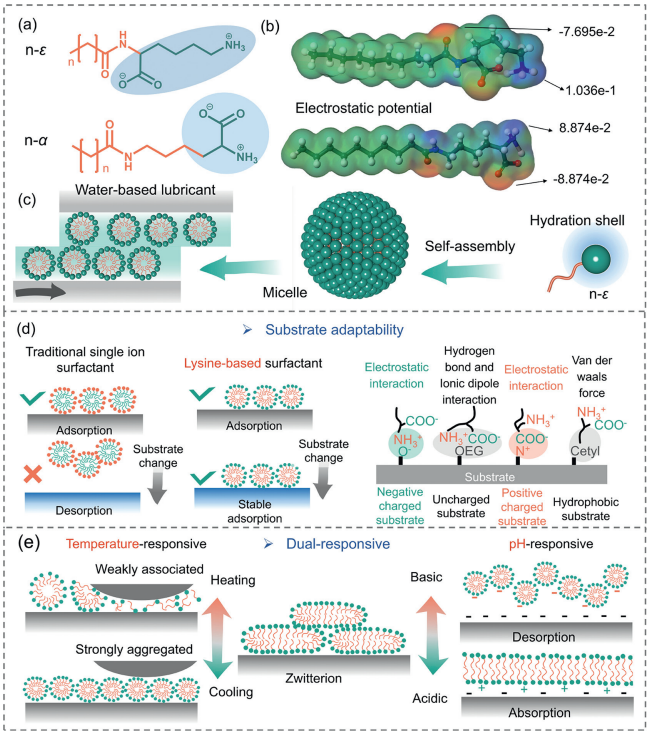


Fig. 1. Schematic diagram of molecular structure, physicochemical properties and lubrication mechanism of LBS. (a, b) Lysine-based surfactant molecular structural formula and electrostatic potential diagram of the head group of two configurations (α and ε, amine cation in the middle of α configuration is closely complexed with carboxylate anion). (c) Schematic diagram of the surfactant gathers in water as micelles, and the micelle molecules are confined to a lubricated state between the glass and the glass. Shearing occurs at the micellar/micellar interface. (d, e) Schematic diagram of the adaption mechanism to changes in substrate materials and double response (temperature and pH response) mechanism of LBS.

The synthetic protocol for LBS is illustrated in Fig. 2a and Fig. S1 (Supporting information). Our strategy employs *tert*–butoxycarbonyl (Boc)-protected lysine derivatives to enable regioselective amidation with NHS-activated fatty acid esters [30], precisely controlling amino group reactivity and ensuring site-specific functionalization. The interactions of 10-ε and 10-α with water molecules were analyzed using density functional theory (DFT). As illustrated in Fig. S2a (Supporting information), the significant interaction between the lysine head group and water molecules indicates that the binding energy of 10-ε with water is greater than that of 10-α. This phenomenon can be attributed to the more facile ionization of the internal salts in 10-ε and the subsequent formation of a hydration layer. The molecular structures of both intermediates and final products were characterized by ^{1}H NMR and FT-IR spectroscopy. The *n*-ε was obtained through the amidation reaction of the carboxyl group of the long-chain acid with the amino group of lysine. The ^{1}H NMR spectrum (Fig. 2b) of *n*-ε shows a characteristic signal at δ 4.36 (-CH-) and the appropriate proportion of methylene integral area within the range of δ 1.25–2.05 (-CH_2-). Besides, the ^{1}H NMR spectrum of *n*-α, and intermediates (NHS ester and Boc-protected *n*-ε) was illustrated in Fig. S3 in Supporting

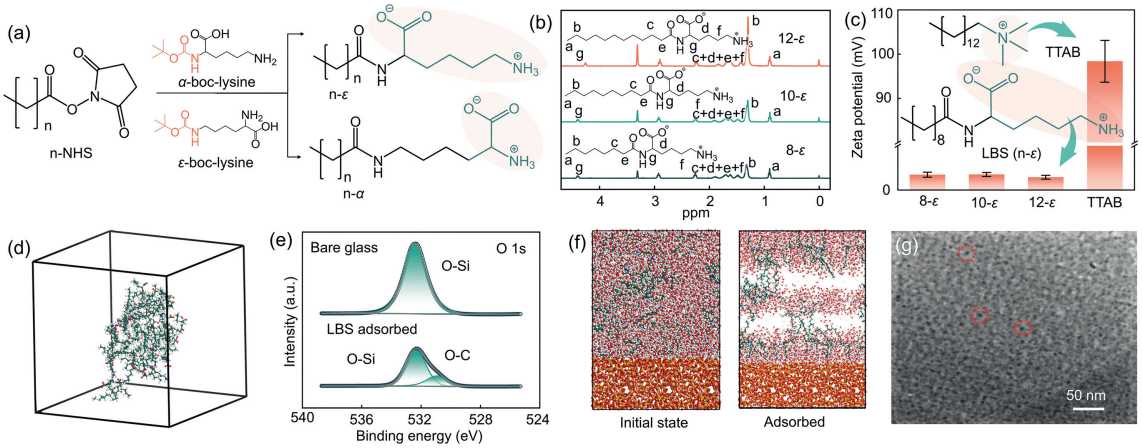


Fig. 2. Synthesis and characterization of LBS: (a) The synthesis process of lysine-based surfactants with two distinct configurations yields an internal zwitterionic salt. (b) ^{1}H NMR characterization of *n*-ε ($n = 8$, 10, 12). (c) Zeta potential of 8-ε, 10-ε, 12-ε, and TTAB. (d) MD simulation of the self-assembly of 10-ε molecules in water (298 K). The C, O, N, and H atoms of 10-ε are colored green, red, blue, and white, respectively. (e) O 1s high-resolution XPS spectrum of bare glass and 10-ε adsorbed. (f) MD simulation of the self-assembly of 10-ε molecules in water on the glass. The C, O, N, Si, and H atoms of 10-ε are colored green, red, blue, yellow, and white, respectively. (g) Cryo-TEM of 10-ε solution.

information. FT-IR analysis (Fig. S2b in Supporting information) of the 10-ε revealed zwitterionic salt formation between protonated amino (-NH_3^+) and carboxylate (-COO^-) groups, though -NH_3^+ stretching vibrations (anticipated 3073.5, 2607.1, 2165.3 cm^{-1}) exhibited attenuated intensity in the 2600.0–2100.0 cm^{-1} range due to charge delocalization effects. Distinct amide I (C=O stretch at 1635.5 cm^{-1}) and amide II (C–N stretch/N–H bend at 1521.2 cm^{-1}) bands confirmed secondary amide formation, while a progression of ~20.0 cm^{-1}-spaced *trans*-conformational -CH_2- rocking vibrations (1350.0–1192.0 cm^{-1}) validated long-chain alkyl structure, consistent with established spectral assignments [31,32]. Thermal stability of 10-α and *n*-ε ($n = 8$, 10, 12) was evaluated using thermogravimetric analysis (TGA). As illustrated in Fig. S4 (Supporting information), the TGA and derivative thermogravimetric analysis (DTG) curves are presented. The results indicate that *n*-ε begins to decompose at approximately 176.5 °C, and the decomposition temperature remains constant regardless of the chain length [33]. Furthermore, the DTG curve reveals that the thermal decomposition temperature of 10-ε is 169.4 °C, suggesting its stability under ambient conditions and highlighting its promising application potential.

Zeta potential measurements of 8-ε, 10-ε, and 12-ε aqueous solutions yielded near-neutral surface charges (3.4 ± 0.6 mV, 3.5 ± 0.5 mV, and 2.9 ± 0.4 mV) [34], values markedly lower than TTAB solutions (98.8 ± 4.7 mV), confirming the zwitterionic headgroup's internal salt configuration through charge neutralization [35] (Fig. 2c). Among the three long-chain LBS, 8-ε exhibited restricted solubility (<2.3 g/L) due to its extended hydrophobic tail's dominance over zwitterionic hydration, while 8-ε's diminished tail cohesion compromised load-bearing capacity. This structure-property relationship identifies 10-ε as the optimal lubricant additive, balancing sufficient hydrophobicity for interfacial film integrity with zwitterionic hydration-driven colloidal stability, achieving an ideal hydrophile-lipophile equilibrium for robust aqueous lubrication under mechanical stress. Molecular dynamics (MD) simulations, as depicted in Fig. 2d, demonstrate that 10-ε undergoes spontaneously self-assembly in aqueous media, transitioning from a disordered molecular state to a well-defined spherical nanoscale micellar structures (Fig. S5 in Supporting information) [36].

This self-organization process is driven by directional molecular alignment, with zwitterionic headgroups oriented outward to maximize hydration and hydrophobic alkyl tails clustered inward, stabilized through non-covalent interactions, including electrostatic interaction cohesion between hydrocarbon chains and electrostatic stabilization of zwitterionic moieties. During this assembly process, the system's energy gradually decreases (Fig. S6a in Supporting information), while radial distribution function analysis (Fig. S6b in Supporting information) confirms water expulsion from the micellar core and preferential accumulation at the hydrophilic surface interface. MD simulations were conducted on the hydrochloride (protonated amine), zwitterionic (inner salt), and sodium salt (deprotonated carboxylate) forms of 10-ε (Figs. S7a and S8 in Supporting information). The results indicated that the zwitterionic surfactant micelles exhibited the highest intermolecular binding energy, potentially leading to superior load-bearing capacity during lubrication. Zeta potential measurements quantified this ionic-state dependence, yielding positive potential (hydrochloride), near-zero potential mV (zwitterionic), and negative potential (sodium salt), consistent with their respective surfactant classifications (Fig. S7b in Supporting information).

The particle size of micelles formed through self-assembly of 10-ε in the concentration of 2.0 g/L was determined, with DLS measurement [37,38] results presented in Fig. S7c (Supporting information). The particle size of the nanoparticles is around 4.2 nm. DSC of concentrated solutions (50 mmol/L) identified chain-length-dependent thermal transitions: 8-ε and 10-ε displayed endothermic peaks at 33.4 °C and 70.9 °C, respectively (Fig. S9 in Supporting information) [39,40]. These findings suggest a significant alteration in the micellar aggregation structure within the solution, possibly transitioning from a multi-layer assembly to a single-layer micelle structure [41]. The longer alkyl chain of 10-ε provides superior thermal stability compared to 8-ε. Due to the excessive hydrophobicity of the alkyl group, the same concentration of the 8-α cannot achieve completely dissolved in water at room temperature, and no significant endothermic peak is observed between 0–100 °C, which is discussed further in Supporting information. Consequently, 10-ε is the most appropriate additive for water-based lubrication. Therefore, the LBS mentioned later refers to the addition of lubricant 10-ε. The ubbelohde viscometer was utilized to measure the relative viscosity of water and a 2.0 g/L 10-ε (LBS) aqueous solution (Fig. S7d in Supporting information). The results indicate that LBS exhibits a viscosity comparable to that of water, suggesting that the formation of micelles has minimal impact on the viscosity of the solution. Compared with other reported types of water-based lubricant additives (including ionic liquids [42], glycerol [43], polymers [44]), the viscosity of LBS is closest to that of water.

In order to explore the substrates with various surface properties (electropositive, electronegative, hydrophobic, hydrophilic) while maintaining a constant load, different surface-modified glasses were selected as the substrate materials for the subsequent work. The water contact angle of the unmodified glass substrate (bare glass) was determined to be 52.17°, reflecting its intrinsic hydrophilic nature. Upon the adsorption of 10-ε molecules onto the surface (denoted as LBS adsorbed), a significant reduction in the water contact angle to 11.46° was observed, suggesting an enhanced hydrophilicity due to the surface modification. This reduction could be attributed to the formation of several molecular layer films on the glass surface after the adsorption of micellar assemblies (Fig. S10 in Supporting information). To further validate the successful adsorption of micelle molecules to the glass substrate, X-ray photoelectron spectroscopy (XPS) analyses were conducted on both the pristine glass and the LBS adsorbed glass. The results, as shown in Fig. 2e, Fig. S11 and Table S1 (Supporting information), provide conclusive evidence of molecular adsorption. Notably, the appearance of the N 1s peak (Fig. S12 in Supporting information), alongside the distinct C–O bond peaks in the C 1s and O 1s spectra confirm the successful adsorption of 10-ε micelle molecules onto the glass substrate. These findings not only validate the efficacy of the adsorption process but also highlighting the potential of LBS in modified surface properties for advanced material applications [45]. To gain deeper insights into the assembly process, molecular dynamics (MD) simulations were performed. These simulations reveal that the head group of the 10-ε molecule initially adsorbs onto the SiO_2 surface (Fig. 2f), followed by the alignment of tail groups and the reorientation of head groups toward each other [46]. The self-assembly transition from a free state result in the formation of an ordered molecular layer structure, as depicted in Fig. S13 (Supporting information). The findings highlight the role of intermolecular interactions in driving the self-assembly process.

Cryogenic transmission electron microscope (cryo-TEM) studies in an aqueous environment (Fig. 2g) further confirmed the aggregate behavior of 10-ε molecules in water demonstrated that the 10-ε molecules aggregated as micelles, with an average size of micelles of ~6.59 nm (Fig. S14 in Supporting information), rather than forming vesicular structures. The rheological behavior of the solution under shear was investigated to elucidate its flow properties. At 25 °C, the viscosity of both water and the LBS solution (the aqueous solution of 10-ε with a mass concentration of 2.0 g/L) remains nearly constant, approximately 1.1 and 1.3 mPa s, respectively, across a broad spectrum of shear rates (Fig. S15a in Supporting information), demonstrating water-like viscosity and classic Newtonian fluid behavior. This rheological profile suggests the lubricant's micellar architecture predominantly comprises discrete spherical or short rod-like micelles lacking structural entanglement, a configuration that fundamentally explains the absence of shear-thinning phenomena [47]. To evaluate the tribological properties of the lubricant at varying surfactant concentrations, glass/glass friction pairs were employed. Prior to testing, both the glass block and glass sphere were treated by plasma to enhance the density of surface oxygen-containing functional groups, thereby promoting micelle adsorption on the substrates. Comprehensive coefficient of friction (COF) measurements conducted under progressively increasing loads (0.1–4.0 N, generating contact pressures from 0.14 GPa to 0.49 GPa (Fig. S15b and Table S2 in Supporting information) [48] provided essential insights into the lubricant's pressure-dependent behavior, with comparative analysis against pure water establishing its superior tribological performance across multiple mechanical stress regimes.

The lubrication performance of surfactant-containing solutions exhibits remarkable concentration dependence, as evidenced by measurements showing the COF of 0.68, 0.12, 0.12, and 0.067 for different concentration of 0.01–1.0 g/L respectively at 0.1 N load. Notably, this lubricity advantage diminishes progressively with increasing mechanical loads due to insufficient interfacial stabilization. When the surfactant concentration in the lubricant is elevated to 2.0 g/L, stable lubrication is achieved across a broad load range from 0.1 N to 4 N. Specifically, the COF for LBS at loads of 0.1–4.0 N are all stable at around 0.064, representing a reduction of approximately 20-fold (92.3 %−94.9 %) compared to pure water (Fig. 3a and Fig. S16 in Supporting information). At lower surfactant concentrations, the adsorbed molecular layers on the friction surface are fewer, resulting in slower re-self-assembly after disruption and diminished load-bearing capacity. These findings underscore the critical role of surfactant concentration in achieving robust and load-resistant lubrication. When subjected to varying shear rates (0.1–10.0 mm/s), the COF remains consistently stable at approximately 0.064, demonstrating that the lubrication performance is independent of sliding speed (Fig. 3b). Under shear conditions, the hydration shell resists compression under applied load, indicating that the hydrated water is not expelled but instead remains in a state of rapid dynamic exchange, effectively functioning as a fluid [49].

Lubricant robustness emerges as a critical performance determinant, given that conventional formulations typically suffer from intrinsically sluggish self-repair kinetics, a limitation causing catastrophic lubricant film failure and irreversible performance decay under operational stresses. Remarkably, LBS exhibits exceptional stability, maintaining consistent lubrication for over 25,000 cycles (over 50,000 s at a velocity of 5 mm/s) under controlled temperature and humidity conditions (Fig. 3c). Throughout the entire friction process, LBS remains stable COF, even after partial disruption of the molecular layer during cycling, the COF in the final cycle stabilizes at ~0.1, highlighting its exceptional long-term stability and self-recovery capabilities as a high-performance lubricant additive. Following the validation of LBS's cyclic stability, its anti-wear properties were further investigated. A detailed analysis of the wear tracks on the glass surface post-friction was conducted using optical microscopy and white light interferometry (Figs. S17a-d in Supporting information). These results provide critical insights into the material's durability and wear resistance, reinforcing its potential as a robust lubricant for demanding applications. In pure water, direct contact between the glass sphere and the glass block results in pronounced wear marks on the glass surface, featuring a deep pit with an average width of 663.68 μm and a depth of 13.44 μm (Fig. S17e in Supporting information). In stark contrast, the introduction of 10-ε molecules significantly mitigates wear; no discernible grooves are observed in the optical microscope image, and only minor scratches aligned with the friction direction are detected in the white light interferometry (WLI) image. This wear reduction is attributed to the adsorption of the lysine zwitterionic head groups of 10-ε molecules onto the frictional surfaces through non-covalent interactions, such as dipole-charge interaction. The micellar molecules form multiple molecular layers on the friction pair's surface, with the charged head groups exposed to the solution firmly anchoring numerous water molecules to create a robust hydration shell [50].

In practical applications, the choice of friction pair materials with varying surface electrical properties is critical. For example, materials such as mica, quartz, and glass typically exhibit negative surface potentials, limiting anionic surfactant adsorption and consequent lubrication efficiency. To explore the adaptability of LBS to various substrate, glass friction pairs with different surface properties were prepared (Fig. S18a in Supporting information). The implementation of variably modified glass surfaces enables precise control of friction loads, ensuring consistent tribological performance across experimental conditions. The negative charged substrate was obtained by plasma treatment of clean glass (glass-O^-), the uncharged substrate was obtained through oligomer

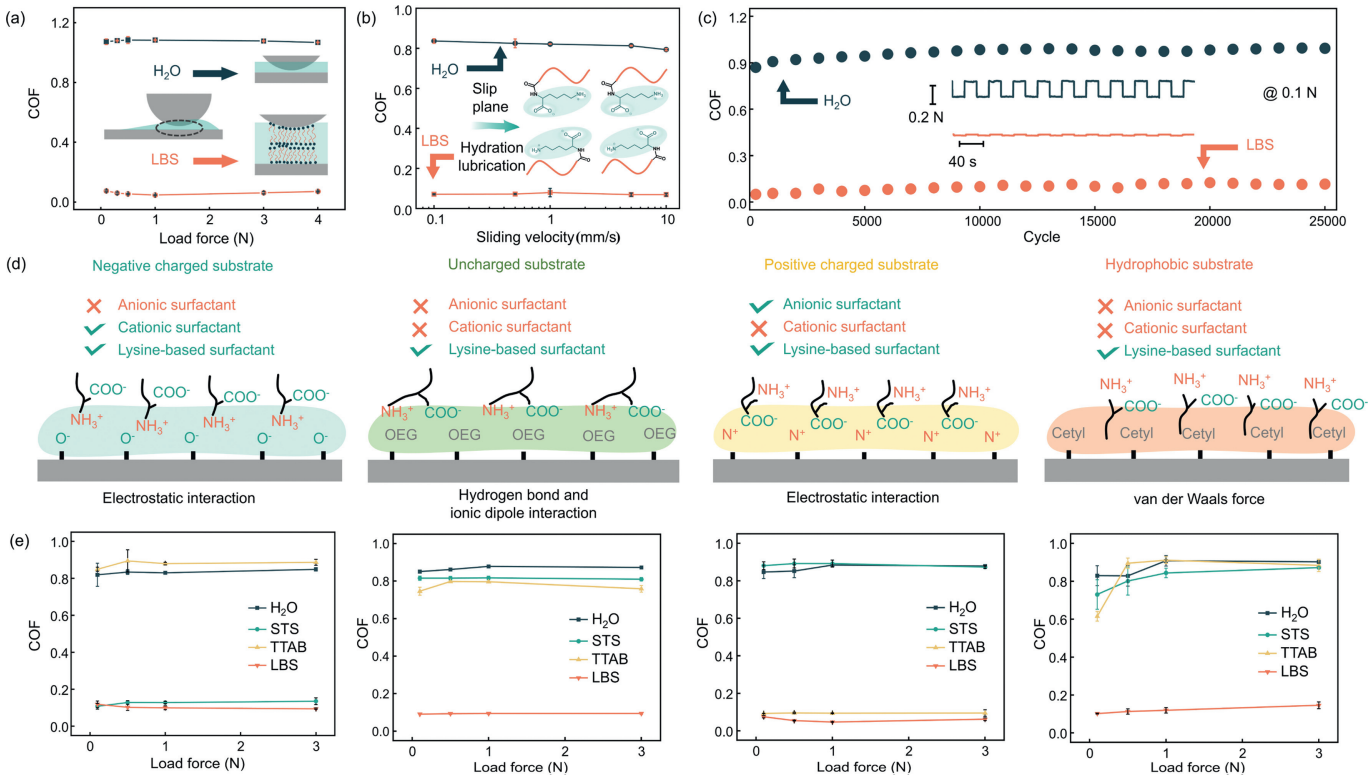


Fig. 3. Lubrication properties of low viscosity lubricants: (a) Effect of applied load force on the COF of H_2O and LBS at velocity of 5 mm/s. (b) Effect of applied sliding velocity on the COF of H_2O and LBS at the load of 1 N. (c) Long-term friction cycling performance of H_2O and LBS at load of 1 N and velocity of 5 mm/s. (d) Scheme of the adsorption behavior of LBS in different substrates (negative charged, uncharged, positive charged and hydrophobic substrate). (e) COF of H_2O, STS, TTAB, LBS.

ethylene glycol trimethoxysilane modified (glass-OEG), the positive charged substrate was obtained through PDADMAC self-assembles layer by layer on glass-O^- and the hydrophobic substrate was obtained through hexadecyltrimethoxysilane treatment (glass-cetyl). The water contact angles of these modified surfaces were 11.5°, 34.3°, 10.8° and 100.9° (Fig. S18b in Supporting information).

Surface characterization revealed a higher oxygen content on the plasma modified glass, higher nitrogen content on the PDADMAC modified glass, higher oxygen and carbon content on the OEG modified glass and higher carbon content on the cetyl modified glass (Fig. S18c and Table S3 in Supporting information) compared to untreated glass, confirming successful modification. To demonstrate the adaptability of LBS to substrates with different surface properties, pure H_2O, anionic surfactants (sodium tetradecyl sulfonate, STS) and cationic surfactants (tetradecyltrimethylammonium bromide, TTAB) of the same elastic chain length were selected and prepared into solutions of the same concentration for comparison. The COF of pure water remains stable at approximately 0.90 on substrates with different surface properties, but different types of surfactants exhibit different lubricating properties on different substrates.

The COF of STS remains similar to that of pure water (approximately 0.89) on the negative charged substrate, indicating no substantial improvement in lubrication performance. Due to electrostatic repulsion, anionic surfactants cannot be adsorbed on negative charged substrate. In contrast, the quaternary ammonia of TTAB and the amino-cationic group of the LBS (Fig. 3d). enables strong adsorption onto negative charged substrate through electrostatic attraction, facilitating the formation of a stable molecular layer. This leads to the significantly reduced COF of cationic surfactant and LBS, stabilizing at approximately 0.095 and 0.054 (Fig. 3e). STS and TTAB can only adsorb onto substrates through electrostatic interactions, significantly limiting their substrate adaptability. For instance, on uncharged surfaces, both surfactants fail to provide effective lubrication due to the absence of electrostatic attraction between their headgroups and the substrate. In contrast, the amino and carboxyl groups in the LBS headgroups can form hydrogen bonds with OEG and adsorb onto the OEG surface *via* ion-dipole interactions. This mechanism enables LBS to maintain a stable COF of approximately 0.092, even on uncharged substrates.

Similar to its behavior on negatively charged substrates, TTAB fails to maintain effective lubrication on positively charged surfaces due to electrostatic repulsion between its cationic headgroups and the substrate. In contrast, both STS and LBS demonstrate stable lubrication performance, with COF maintained at approximately 0.110 and 0.089, respectively. This enhanced performance arises from the strong adsorption of sulfonic acid groups (in STS) and carboxylate anions (in LBS) onto the charged substrate surface. In contrast to hydrophilic substrates, surfactants exhibit altered aggregation behavior on hydrophobic surfaces, with their tail groups oriented toward the substrate. While van der Waals interactions theoretically enable all surfactant types to adsorb onto hydrophobic substrates, our experiments revealed that TTAB and STS fail to provide stable lubrication under these conditions. These single-ion surfactants maintain effective lubrication only briefly (tens of seconds) under minimal loads before film failure occurs. This limitation likely stems from the inherently weak binding affinity between their head groups, which prevents the formation of a robust multimolecular lubricating layer. In comparison, LBS demonstrates superior stability due to synergistic hydrogen bonding and electrostatic interactions between its amino and carboxyl groups, facilitating the formation of a durable, well-organized surface layer (COF maintained at approximately 0.10).

Unlike conventional surfactants (STS and TTAB) whose adsorption is limited to specific surface charges, LBS demonstrates universal adaptability, maintaining stable lubrication (COF~0.05–0.10)

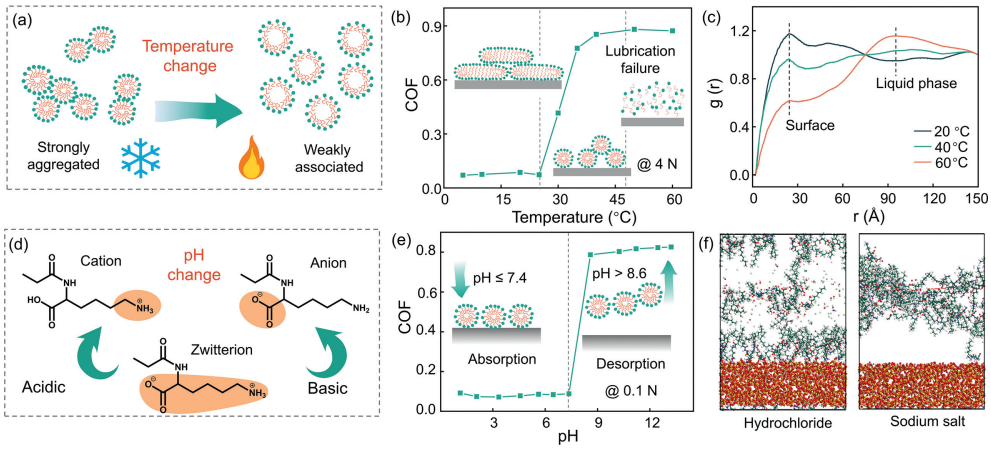


Fig. 4. Dual responsiveness of low viscosity lubricants: (a) Schematic diagram of LBS temperature response. (b) COF of the LBS upon alternately changing the temperature from 5 °C to 60 °C. (c) Radial distribution function of 10-ε molecule and friction pair (SiO_2). (d) Schematic diagram of LBS pH response. (e) COF of the LBS upon alternately changing the pH from 1 to 14. (i) MD simulation of the self-assembly of hydrochloride, and sodium salt molecules in water on the glass. The C, O, N and H atoms are colored green, red, blue and white. The Cl^- and Na^+ are colored light green and purple.

across negatively charged, positively charged, neutral, and hydrophobic substrates through synergistic electrostatic, hydrogen bonding, and ion-dipole interactions. Due to the weaker interaction between LBS and hydrophobic substrates (van der Waals forces) compared to non-charged substrates (hydrogen bonds and ionic dipole interactions), the COF of hydrophobic substrates (0.100) is slightly higher than that of non-charged substrates (0.087).

The dual-responsive behavior of the lubricant was evaluated in the negative charged substrate. As previously discussed, the aggregation structure of micelles in the LBS lubricant exhibits temperature-dependent reversibility (Fig. 4a). This structural adaptability enables a dramatic, temperature-controlled COF switching from low friction (0.076 at 20 °C) to high friction (0.78 at 60 °C), a 10-fold dynamic range maintained through multiple reversable thermal cycles (Fig. S19 in Supporting information). The stability of micelles in the lubricant diminishes with increasing temperature. Under a load of 4.0 N, the COF for LBS at temperatures of 5, 10, 20, 25, 30, 35, 40, 50, and 60 °C is 0.071, 0.075, 0.086, 0.073, 0.416, 0.776, 0.853, 0.881, and 0.873, respectively (Fig. 4b). With the increase of temperature, the micelle becomes loose and the load-capacity decreases [51,52]. Notably, the lubrication performance begins to deteriorate at temperatures above 30–35 °C, with the COF reaching its maximum at 50 °C. To further elucidate the underlying mechanisms, confined shear molecular dynamics simulations were conducted to examine the adsorption dynamics of LBS on the glass substrate during the friction process (Fig. 4c). The surfactant molecules initially adsorb onto the friction pair, upon applying a load of 0.42 GPa (4 N) at 20 °C [53]. When the molecular layer is disrupted, free micelle molecules in the solution rapidly re-adsorb onto the friction pair, forming a new molecular layer. After 600 ps of shearing, the lubrication film remains largely intact, demonstrating its resilience and self-repairing capability under shear stress. However, as the temperature rises, the density of LBS adsorbed at the interface diminishes (within the range of 20–30 Å, corresponding to 0–10 Å from the interface), while the density of free micelle molecules in the liquid phase increases. This shift results in a reduction in the compressive resistance of the lubricant film at elevated temperatures (Fig. S20 in Supporting information).

In neutral environments, it maintains zwitterionic character ($-NH_3^+/-COO^-$), transitioning to an anionic surfactant ($-NH_2/-COO^-$) under alkaline conditions while retaining anionic characteristics ($-NH_3^+/-COOH$) in acidic media (Fig. 4d). The lubricant exhibits rapid and reversible transformations in surfactant properties in response to pH variations, as depicted in Fig. S21 (Supporting information). At a pH of approximately 3.00, the COF is around 0.083, while at a pH of 8.00, the COF increases significantly to approximately 0.87, representing a 10-fold change. This switchable behavior is repeatable over multiple cycles, demonstrating the durability and reversibility of the lubrication effect. A pronounced increase in COF is observed between pH 7.36 and 8.59 (Fig. 4e and Fig. S22 in Supporting information), which is attributed to the rapid switching of the electrical properties of the 10-ε molecule's head group in response to pH changes. When the friction pair surface is negatively charged, only cationic and zwitterionic head groups can effectively adsorb and self-assemble into a lubricating film, whereas anionic surfactants fail to adsorb in sufficient quantities to form such films. This pH-responsive behavior underscores the adaptability of LBS in modulating lubrication performance under varying chemical conditions.

Molecular dynamics simulations demonstrate that both the hydrochloride and zwitterionic forms of LBS can efficiently adsorb onto the substrate surface and self-assemble into well-defined molecular layer structures (Fig. 4f and Fig. S23 in Supporting information). In contrast, the sodium salt form of LBS shows negligible adsorption on the friction pair surface, with a substantial fraction of micelle molecules remaining freely dispersed within the lubricant. This distinct adsorption behavior is the key driver behind the pH-responsive lubrication properties of LBS, highlighting its ability to modulate surface interactions and self-assembly in a pH-dependent manner.

In summary, we have developed a smart lubricant comprising water and a functional additive (LBS), which integrates lubricating stability, substrate adaptability, thermal and pH responsiveness, and low viscosity into a single system. LBS form a lubricating film on negative charged substrate, uncharged substrate, positive charged substrate and hydrophobic substrate surfaces through multiple interaction forces with substrate, which include electrostatic interaction, hydrogen bond and ionic dipole interaction and van der Waals force. Besides, with a viscosity comparable to water, this lubricant enhances lubrication and load-bearing performance without significantly increasing viscous dissipation. By exploiting heat-induced changes in micelle aggregation structures, the lubricant achieves a reversible, 10-fold modulation of the COF through temperature variation. Furthermore, pH adjustments that influence the zwitterionic head group enable a 10-fold change in COF, allowing precise control over interfacial friction interactions. We anticipate that this biocompatible, low-viscosity smart lubricant

will find broad applications in materials science and chemistry, offering a versatile solution for advanced lubrication challenges.

Declaration of competing interest

The authors declare that they have no known competing financial interests or personal relationships that could have appeared to influence the work reported in this paper.

CRediT authorship contribution statement

Yihan Fu: Methodology, Investigation, Formal analysis, Data curation, Conceptualization. **Xinyi Wang:** Data curation. **Sen Li:** Data curation. **Weifeng Lin:** Investigation, Funding acquisition, Formal analysis, Data curation, Conceptualization. **Mingjie Liu:** Supervision.

Acknowledgments

This research is supported by the Beijing Natural Science Foundation (No. L244035), the National Science Fund for Distinguished Young Scholars (Overseas, Nos. KZ37114301, KZ37125801), the Funds of the Natural Science Foundation of Hangzhou (No. 2024HZY0311), and the Foundation of National Center for Translational Medicine (Shanghai) SHU Branch (No. SUITM-202401). The authors acknowledge the facilities, and the scientific and technical assistance of the Analysis & Testing Center, Beihang University. We are grateful to the Bianshui Riverside Supercomputing Center (BRSC).

Supplementary materials

Supplementary material associated with this article can be found, in the online version, at doi:10.1016/j.cclet.2025.111991.

References

[1] J. Li, J. Li, L. Jiang, et al., Langmuir 35 (2019) 11108–11113.
[2] J. Yang, K. Wang, Y. Zheng, et al., Angew. Chem. Int. Ed. 61 (2022) e202202128.
[3] Y. Zhang, W. Lin, Chin. Chem. Lett. 36 (2025) 110566.
[4] W. Lin, J. Klein, Acc. Mater. Res. 3 (2022) 213–223.
[5] R. Goldberg, A. Schroeder, G. Silbert, et al., Adv. Mater. 23 (2011) 3517–3521.
[6] C. Du, T. Yu, X. Sui, et al., Adv. Mater. 37 (2024) 2413781.
[7] L. Wang, L. Zhang, C. Du, et al., ACS Nano 18 (2024) 34288–34298.
[8] S. Ma, L. Liu, W. Zhao, et al., Nat. Commun. 16 (2025) 398.
[9] J. Zhang, Y. Meng, Friction 3 (2015) 115–147.
[10] T. Han, W. Cao, Z. Xu, et al., Sci. Adv. 9 (2023) eadf3902.
[11] J. Li, J. Luo, Adv. Mater. Interfaces 5 (2017) 1700802.
[12] H. Gu, T. Hirayama, N. Yamashita, et al., Tribol. Int. 188 (2023) 108881.
[13] F. Yan, L. Hu, Z. Ji, et al., Angew. Chem. Int. Ed. 63 (2024) e202318926.
[14] H. Feng, Z. Ma, Y. Zhang, et al., Macromol. Mater. Eng. 305 (2020) 2000135.
[15] Q. Wei, M. Cai, F. Zhou, W. Liu, Macromolecules 46 (2013) 9368–9379.
[16] Y. Cao, N. Kampf, J. Klein, Langmuir 35 (2019) 15459–15468.
[17] X. Ge, J. Li, C. Zhang, et al., ACS App. Mater. Interfaces 11 (2019) 6568–6574.
[18] R. Zhang, S. Ma, Q. Wei, et al., Macromolecules 48 (2015) 6186–6196.
[19] G.R. Quezada, R.E. Rozas, P.G. Toledo, J. Phys. Chem. C 121 (2017) 25271–25282.
[20] N. Kampf, C. Wu, Y. Wang, J. Klein, Langmuir 32 (2016) 11754–11762.
[21] S. Cowie, P.K. Cooper, R. Atkin, H. Li, J. Phys. Chem. C 121 (2017) 28348–28353.
[22] Z. Li, Q. Liu, Q. Li, M. Dong, Nano Res. 16 (2023) 1096–1100.
[23] J. Kang, X. Zhang, X. Yang, et al., Adv. Mater. 35 (2023) 2307705.
[24] Z. Zhang, C. Qin, H. Feng, et al., Nat. Commun. 13 (2022) 6964.
[25] J. Kang, X. Yang, X. Yang, et al., Chin. Chem. Lett. 35 (2024) 109297.
[26] X. Li, B. Wu, S. Sun, P. Wu, Adv. Mater. 36 (2024) 2411273.
[27] S. Chen, H. Sun, J. Liu, et al., Mater. Horiz. 11 (2024) 1668–1678.
[28] T. Gao, J. Li, W. Wang, J. Luo, Friction 11 (2022) 513–523.
[29] W. Lin, N. Kampf, J. Klein, ACS Nano 14 (2020) 7008–7017.
[30] J. Liu, S. Guo, Z. Li, et al., Colloids Surf. B 73 (2009) 36–41.
[31] Z.A. Wang, Y. Kurra, X. Wang, et al., Angew. Chem. Int. Ed. 56 (2017) 1643–1647.
[32] W. Xue, X. Lin, L. Xu, et al., Adv. Mater. 35 (2023) 2304594.
[33] V. Sharma, C. Bhatia, M. Singh, et al., J. Mol. Liq. 308 (2020) 113006.
[34] F. Sharifi, M. Jahangiri, I. Nazir, et al., J. Colloid Interface Sci. 585 (2021) 126–137.
[35] Q. Liu, Z. Chen, Y. Yang, Cem. Concr. Compos. 124 (2021) 104253.
[36] M. Ahmadi, Q. Hou, Y. Wang, Z. Chen, Adv. Colloid Interface Sci. 283 (2020) 102242.
[37] D. Li, X. Wei, W. Xue, et al., ACS Appl. Nano Mater. 5 (2022) 9344–9355.
[38] Y. Zhang, W. Song, J. Geng, et al., Nat. Commun. 7 (2016) 11649.
[39] L.J. Endter, Y. Smirnova, H.J. Risselada, J. Phys. Chem. B 124 (2020) 6775–6785.
[40] Y. Guo, S. Apergi, N. Li, et al., Nat. Commun. 12 (2021) 644.
[41] R.A. Gonçalves, P. Naidjonoka, T. Nylander, et al., RSC Adv. 10 (2020) 18025–18034.
[42] Q. Yu, G. Huang, M. Cai, et al., Tribol. Int. 95 (2016) 55–65.
[43] A. Trajkovski, S. Matkovič, N. Novak, et al., Tribol. Int. 192 (2024) 109173.
[44] T. Poláček, P. Šperka, I. Křupka, Friction 12 (2023) 164–173.
[45] M. Tang, S. Deng, D. Xu, et al., J. Mater. Sci. Technol. 223 (2025) 287–307.
[46] M.B. Boggara, M. Mihailescu, R. Krishnamoorti, J. Am. Chem. Soc. 134 (2012) 19669–19676.
[47] Z. Chu, Y. Feng, Langmuir 28 (2011) 1175–1181.
[48] J. Deng, R. Wei, H. Qiu, et al., Carbohydr. Polym. 330 (2024) 121821.
[49] W. Lin, R. Mashiah, J. Seror, et al., Acta Biomater. 83 (2019) 314–321.
[50] T. Wang, Y. Wang, X. Wang, et al., ACS Nano 18 (2024) 33468–33478.
[51] S. Feng, Y. Liu, J. Li, et al., Langmuir 36 (2020) 13477–13484.
[52] R. Sorkin, N. Kampf, Y. Dror, et al., Biomaterials 34 (2013) 5465–5475.
[53] Y. Li, S. Wang, B. Arash, Q. Wang, Carbon 100 (2016) 145–150.